Statistics and variability of the altitude of elves

Oscar A. van der Velde and Joan Montanyà

Lightning Research Group, Electrical Engineering Department, Technical University of Catalonia.

Colon 1, 08222 Terrassa (Barcelona), Spain

contact: oscar.van.der.velde@upc.edu

Key points:

Elves appear mainly November through February over the Bay of Biscay and western Mediterranean Sea

Elve altitudes are determined combining optical methods and lightning location

Nightly mean elve altitudes vary between 83 and 93 km and also vary over a timescale of hours

Abstract

From June 2008 to January 2016 nearly 800 elves have been recorded by a low-light camera in northeastern Spain. Elves occur in this region mainly over the lower-topped cold airmass maritime thunderstorms, peaking from November to January. Cloud-to-ground strokes still produce elves when maritime winter storms are carried inland, suggesting the cold season thunderstorm charge configuration favors strokes with large electromagnetic pulses. Altitudes of 389 elves were determined using optical data combined with a lightning location network. The overall median altitude was 87.1 km, near the typical OH airglow height, but average heights during individual nights ranged between 83 and 93 km. The lower elve nights (~84 km) occurred during slightly elevated geomagnetic conditions (Kp >3-, ap-index >10). Elve altitude often shifts by several kilometers during the night, apparently in response to changing background conditions in the upper mesosphere.

1. Introduction

Elves are transient optical emissions in the upper D-region ionosphere [*Inan et al*. 1991; *Taranenko et al.*, 1993] in the shape of donut-like rings of a few hundred kilometers wide, centered above cloud-to-ground lightning strokes that emit very strong electromagnetic pulses (EMP). They are produced by excitation of the first and second positive bands of nitrogen molecules (N_2) impacted by free electrons energized by the strong EMP [*Taranenko et al.*, 1993; *Marshall et al.*, 2010; *Kuo et al.*, 2012]. Long-lasting perturbations of electron density have been observed after elves [*Haldoupis et al.,* 2012]. Models have been built which successfully reproduce aspects as the shape, expansion speed and the location and intensity of optical emissions of elves in response to lightning impulse and vertical profiles of electron density and neutral species [e.g. *Inan et al.* 1996; *Barrington-Leigh et al.,* 2001; *Kuo et al.,* 2007; 2012; *Marshall et al.,* 2010].

The earliest observations of elves were made from the space shuttle [*Boeck et al.,* 1992] and revealed a superposition with the hydroxyl (OH) airglow layer between 85 and 90 km altitude [e.g. *Baker and Stair*, 1988], corroborated by later space missions [*Israelevich et al.,* 2004; *Huang et al*.,

2010], although a precise altitude estimation from limb observations is complicated by the geometry. Elves have subsequently been reported from the ground [e.g. *Fukunishi et al.*, 1996; *Barrington-Leigh and Inan*, 1999; *Barrington-Leigh et al.,* 2001; *Takahashi et al.*, 2003; *Neubert et al.,* 2008; *Soula et al.,* 2010; *Montanyà et al*., 2010; *van der Velde et al.*, 2011]. Satellite-derived global climatologies by *Chen et al.* [2008; 2014] show elves to be most frequent over the tropical seas.

The goal of this paper is to establish statistics of the altitude of elves using a large dataset of ground-based observations (continued since *van der Velde et al.* [2011]). In principle, the altitude of elves depends on characteristics of the very low frequency (VLF) lightning impulse, the increase of electron density with height, and the decrease of neutral density with height. The energy required for free electrons to excite the positive bands of N_2 can only be reached where electron densities and mean free paths are sufficiently large and where the plasma frequency allows an electric field to penetrate. Studies of nighttime reflection heights using sferics in the extremely and very low frequency range report variations between 82 and 87 km [e.g. *Han and Cummer*, 2010; *Lay and Shao*, 2011; *Maurya et al.*, 2012] which roughly correspond to the nocturnal 82–92 km altitude range of the electron density increase from 10^7 to $>2 \cdot 10^9$ m^{-3} in profiles taken by rocket probes summarized by *Friedrich and Torkar* [2001]. The steep electron gradient is often discussed referring to hydrated cluster ions below 85 km which scavenge free electrons due to their large electron recombination coefficient [e.g. *Reid*, 1970; *Sugiyama*, 1988]. These cluster ions also play a role in the recovery from electron perturbations produced by elves [*Gordillo-Vázquez et al*., 2016]. A relation between the electron density profile and OH airglow emissions is currently not known.

2. Methods and measurement errors

74

75 To find elve altitude we combine the elve's central elevation angle retrieved from star-
76 calibrated camera images with the corresponding lightning CG stroke location providing the
77 distance using spherical Earth geometry explained in detail in supporting information S1. The steps
78 of the procedure are detailed in S2.

79 Elve images were obtained with a Watec 902H2 Ultimate 1/2" CCD camera located in
80 northeastern Spain (41.67°N, 1.85°E, 190-270m), in almost all cases with a 12mm F0.8 lens
81 (producing an image with a 31° angle wide view horizontally), occasionally with a 0.7x wide angle
82 converter (43°). A UTC time stamp accurate to 1 ms was inserted into 20 ms exposures by a device
83 using timing from the Global Positioning System. UFOCapture software was used to detect events
84 in the video stream with the most sensitive thresholds possible with respect to the image noise level.
85 As the camera system did not continuously monitor the entire sky and detection of elves is
86 imperfect given the imager limitations, choices of the observer, interference by other triggers (bats,
87 airplanes) and partial obstruction by clouds or hills, the data can only roughly approximate the true
88 frequency of occurrence of elves.

89 For image analysis an image containing the mean value of the pixels over all frames was
90 calculated for each elve video clip – excluding the frame containing the event. This background
91 image was subtracted from the event image to remove luminosity gradients or clouds and the
92 resulting event-only image was stretched for contrast. The background image was used to fit stars in
93 a sky charts software to fix the view. This was done each time the camera view changed.
94 Subsequently, azimuth and elevation angles of elve centers were manually read out at the cursor.
95 The precision of the star fix combined with the precision of readout of the hole center are accurate
96 to within 15 arcseconds, with far events having smaller readout variation because of the smaller
97 elve hole. This has been tested by repeating star fixes and elevation readouts: a night with 8 elves
98 around 400 km distance resulted in a mean difference in elevation of -1.3 arcminutes and a standard

99 deviation of 8 arcminutes between new and old readouts. At typical elve distances the optical error
100 results in a -1 to +1 km altitude uncertainty range for individual events.

101 The conversion of elevation to altitude is described by *van der Velde* [2008] and assumes a
102 spherical Earth, is based on great circle path between observer and lightning stroke and also
103 considers camera altitude. It is included here as supporting information S1. Because the elevation
104 readout was performed on the geometric center of the elliptical hole of the two-dimensional elve
105 projection, the perspective effect causes the far half of the elve hole to be more compressed in
106 elevation angles than the near half. The altitudes presented here are corrected for this effect,
107 assuming a hole radius of ~35 km [*Blaes et al.*, 2014]. The correction function amounts to -2 km for
108 elves at 200 km distance, -1 km at 300 km, -0.5 km at 450 km and -0.2 km at 800 km distance. The
109 effect on the correction of a 10 km difference in hole radius is less than 0.5 km in altitude for events
110 beyond 300 km distance. Supporting information S3 includes an example that confirms the
111 precision of the optical analysis by independently determining the altitude for the same elve
112 recorded by two cameras at different altitudes (190m and 2880 m).

113 Cloud-to-ground lightning flashes responsible for the elves were located using the "Linet" low-
114 frequency time-of-arrival lightning detection network [*Betz et al.*, 2004; 2009]. The location
115 accuracy is in principle better than 500 meters, but a comparison between elve and stroke azimuths
116 and corresponding lateral distances shows differences of a few kilometers to 10 kilometers and
117 more. There are three factors contributing to this difference: 1) The lightning signal detection and
118 locating algorithms; 2) The projection of an elve by a tilted return stroke dipole antenna pattern or
119 significant intracloud component [*Marshall et al.,* 2010], and 3) The readout precision of the elve
120 center azimuth (~0.5°).

121 Elve-producing strokes are the ones that produce the strongest EMPs of all lightning, and
122 waveforms in low frequency receivers can exhibit a wave train not seen in normal strokes. This can
123 cause multiple triggers on different parts of the waveform in different detection time slots, resulting

in multiple locations as well as ambiguity in reported polarity and peak current. Besides the main stroke, elve-producing strokes can be preceded by intense breakdown processes which can also cause triggers. These issues with the detection of this exceptional class of strokes are not unique to the Linet network, however. For quality control, we rejected strokes with lateral differences of more than 10 km (~ >1° azimuthal difference), but this still allows a distance error along the line of sight, where 10 km amounts to ~3.5 km in altitude for elves at 250 km distance and 1.5 km for those at 600 km. The median lateral distance for accepted strokes is 2.7 km, while it is 14.7 km for rejected detections. The error is in part natural, as some deviation in azimuth is expected in case of elves projected by return stroke channels tilted away from the vertical. So, in half of the cases the Linet location accuracy and tilted EMP projections contribute to an altitude error of less than ±1 km.

Between June 2008 and February 2016, 795 elve events were recorded by the camera in northeastern Spain. It is supplemented by 21 elves recorded at Pic du Midi (42.94°N, 0.14°E, 2877m) in the summers of 2010 and 2015. Of these 816 events, 545 events were suitable for optical analysis. Of those, Linet provided a plausibly located CG stroke detection in 389 cases.

3. Results

3.1 Peak currents of elve-producing strokes

A boxplot of the peak currents of the optically verified Linet strokes for the elves is displayed in Figure 1a. The whiskers extend to the 2% and 98% percentiles of the distribution, corresponding to 130 kA and 370 kA. The median is 228 kA. Excluded were any detections of strokes weaker than 70 kA, as we believe that these were detections of other processes in the same flash under the elve's central azimuth, with the main elve-producing stroke undetected. The polarity indicated by the

149 Linet network is almost even between negative and positive (51% to 49%), and their statistical
150 distributions are also very close.
151
152 3.2 Elve locations
153
154 Figure 1b shows that the majority of elves occur over the Bay of Biscay (Atlantic Ocean) and
155 over the Mediterranean Sea. While elves were observed mainly from November through January
156 from the central Catalonia location, the camera at Pic du Midi usually records elves throughout the
157 entire winter half year, when cold airmasses over warm sea water provide a source of convective
158 available potential energy for thunderstorms (as opposed to the cold land). During summer, storms
159 initiate mainly over land and often produce sprites if they continue to grow at night [e.g. *Neubert et*
160 *al.*, 2008; *Soula et al.,* 2009, *Bór*, 2013; *van der Velde et al.,* 2014]. However, these summer
161 thunderstorms monitored by the same camera setups rarely produce elve detections, even if they
162 move over sea, as illustrated by the cases discussed by *Füllekrug et al.* [2013] and *Soula et al.*
163 [2014].
164 Several tracks of individual elve-producing winter thunderstorms can be noticed over the Bay
165 of Biscay. Elve CGs continue to be produced over land (southwestern France and the north coast of
166 Spain) as such storms move onshore. While not shown here, sprites are much less frequent than
167 elves over the Bay of Biscay compared to the Mediterranean where the warmer and more humid air
168 near the surface harbors energy for thunderstorms to grow into larger clusters allowing lightning to
169 tap into larger reservoirs of positive charge for triggering sprites, which is not a requirement for
170 elve-producing discharges.
171 A relative lack of elves is apparent in a zone of a few hundred kilometers wide from the
172 Spanish and French coastlines over the western Mediterranean Sea. However, given the various
173 reasons explained before, an absence of elves observed does not necessarily mean they did not

174 occur. The map does resemble very well the frequency of "winter lightning" under the criterion of
175 temperatures below -10°C at 700 hPa [*Montanyà et al.*, 2016], and a similar distribution is shown
176 for estimated elve producing strokes by *Blaes et al*. [2016] over the western Mediterranean region.
177 However, we do observe relatively more elves over the Bay of Biscay in comparison to their map.
178 Thunderstorms are frequent and often very active with high flash rates in the Balearic Sea
179 after the entry of a cold front into the Mediterranean in autumn. However, elves seem to be
180 observed more frequently with limited instability, small cells and reduced flash rates, as is typical
181 on the Atlantic side of the Iberian Peninsula. Just having any thunderstorm over sea in the right
182 season is no guarantee for elve production. It may still take hours, hundreds of flashes and tens of
183 sprites before an elve appears over maritime winter thunderstorms, for example on 5-6 and 6-7
184 December 2015, observed from Pic du Midi over the Mediterranean Sea. It was also the case in
185 *Soula et al.* [2010]. It strongly suggests a certain cloud charge configuration and type of lightning
186 flash is required for elves, as is the case for sprites.
187
188
189 3.3 Elve altitude
190
191 Figure 1c shows that the determined altitudes of the winter elves range between 80 and 96 km
192 with 25th percentile, median and 75th percentile values for the total population of 85.2 km, 87.1 km
193 and 88.6 km, respectively. The standard deviation is 2.42 km. However, elve altitudes do vary from
194 night to night (Figure 2). The mean standard deviation per night is 1.57 km, significantly smaller.
195 The mean altitudes for nights with 7 or more elves vary between 83.4 km and 90.0 km. The 95%
196 confidence intervals of these mean values are indicated in Figure 2 by red triangles.
197 It could be noted that the map in Figure 1b shows higher altitudes over the Mediterranean Sea
198 (mean 87.8 km) than over the Bay of Biscay (86.2 km). This is unlikely to be a regional effect.

Before the inclusion of 5 November 2014, 17 January 2015 and 12 January 2016 events over the Bay of Biscay (collective mean of 84.3 km), the mean altitude in that region was in fact 87.6 km, virtually the same.

The markedly lower altitude nights mentioned above may be related to the solar cycle. The sunspot minimum occurred in the years 2008-2009 and the maxima appeared in late 2011 and early 2014 with a decline over 2015 and 2016. The years 2008-2011 contributed more elves with altitudes above the mean, whereas late 2013 to early 2016 contributed more elves below the mean altitude. In fact, these nights were all associated with ap-index values between 10 and 30 nT (marked in grey in Figure 2), indicating only slightly disturbed global geomagnetic conditions (Kp index > 3-). Supp. Info. S6 shows slight negative correlations between elve night median altitude (35 nights), the ap-index ($R^2 = 0.32$) and the F10.7 cm daily solar radio flux ($R^2 = 0.08$).

To investigate the possibility of seasonal altitude differences we also considered two summer nights with significant elve activity, observed with a similar camera system installed on Pic du Midi. A storm over the Rhone Valley north of Avignon in France produced 9 elves and a number of sprites (as well as combined events) in the early hours of 20 August 2010. The mean altitude was 93.3 km with a standard deviation of 2.4 km, significantly higher than the other cases. The other night of 6-7 June 2015 with 11 elves over the Aosta Valley in the Alps resulted in a more typical 87.2 km as mean altitude and 2.1 km standard deviation (for 7 events with a succesful CG detection). So, while one case appears to be anomalously high, more cases are needed to establish seasonal differences. There are a few isolated elves in May and June which fall close to the peak of the distribution.

It is also worth noting that there is no correlation between elve altitudes and the peak current of corresponding lightning strokes in the Linet data (see Figure S4 in the Supporting Information).

3.4 Temporal and spatial altitude changes

As elve altitude is affected by the electron density profile, the transition from daytime to nighttime conditions may be detectable for elves occurring in the hour after sunset and before sunrise. A time-altitude graph of elve events labeled by year is included as Figure S5 (Supp. Information). While elve altitudes are lowest at nightfall with a median of 86.2 km before 1930 UTC (Atlantic) or 1900 UTC (Mediterranean), the number of nights (2) with elves in this time interval is so small that one cannot draw conclusions from this. The other periods of the night large altitude differences between nights which dominate over nocturnal evolution, although the years 2014-2016 are mainly responsible for broadening the altitude range.

On the other hand, during individual nights with large numbers of elves, changes in altitude over time and space are often observed (Figure 3). One use of the graphs is to identify any bias in altitude according to observing distance (there is none). The graphs also show trails and tight clusters of elves when produced by one thunderstorm cell. For the Atlantic cases (the two columns at the right), the camera was looking into the direction of the northwesterly flow carrying the cold airmass thunderstorms towards the Iberian Peninsula and French coasts, so that distance of elves from the camera is decreasing with time. For the Mediterranean cases (left column) it is the reverse.

There appears to be less variability within traces than there is between traces or clusters occurring at different times. This suggests that individual elve altitude errors are smaller than the changes during the night, particularly when changes are as large as 2-3 km. The variation can be observed mainly over the time domain, and is of similar magnitude as reported by studies of reflection height by tweek studies [e.g. *Han and Cummer*, 2010]. It can be noted that the altitude changes occur at seemingly random moments during the night and in either direction. Transitions from lower to higher occurred at: 0300 UTC (*a*), 2300-0100 UTC (*f*); from higher to lower: 2030 UTC (*c*), 0300-0400 UTC (*d*), 0230 UTC (*e*). Within individual storm traces there is no evidence of a systematic influence of the lingering ionization produced by previous elve-producing strokes on

the altitude of a next one. We also do not see any difference between nights with most elves displaying gravity wave patterns (*b*, *e* and *f*) versus nights with smooth elves (*a*, *c* and *d*).

4. Discussion

Elves are observed mainly during the autumn and winter over the western Mediterranean Sea and the Bay of Biscay, similar to elve occurrence in Japan [*Takahashi et al.*, 2003]. They are also produced by CG strokes over land as the storms move ashore and dissipate. Peak currents reported by the Linet network for the detected elves range mainly between 130 kA and 370 kA (2% and 98% percentiles) with a median of 228 kA. This is well above the threshold of 88 kA [*Blaes et al.*, 2016] for elves to be detectable with 50% probability by photometers, which are more sensitive systems than the camera used here. The high conductivity of sea water compared to land should help in attaining high peak currents [e.g. *Said et al.*, 2013], and may be generally important as cold season thunderstorms occur mainly over sea, but it is not the only determining factor. *Chen et al.* [2014] show that the ratio of energetic to normal lightning, in our case over the Western Mediterranean Sea indeed changes with the season (note a mismatch between their figure captions and the well-known global lightning climatology).

As elves are rarely observed in summer thunderstorms and certain maritime autumn thunderstorms with our cameras, it is an indication that the meteorological regime and electrical cloud characteristics are an important factor for high rates of elve-producing CG strokes in the cold season, be it over sea or land. Elves have been detected in summer as well in the USA using photometers and high-speed cameras, but often have insufficient brightness to be detected by

conventional low-light video cameras [e.g. *Newsome and Inan*, 2010]. This means either that large peak current strokes occur less frequently or the optical excitation is less effective. As an example of the latter, the modeling of *Taranenko et al.* [1993] and *Marshall et al.* [2010] produces stronger emissions for tenuous electron density profiles. A denser electron profile means a lower reflection altitude at a larger neutral density, resulting in reduced electron energies, which need to be compensated by stronger lightning impulses. But also a too weak electron density will limit the emissions. Another factor that could come into play are increases [*Han and Cummer*, 2010] or decreases [*Shao et al.,* 2013] of D-region electron density produced by thunderstorms in proportion to their flash rates. Summer thunderstorms generally produce much higher rates of negative cloud-to-ground flashes and intracloud flashes because larger amounts of water vapor and buoyancy are available.

The overall median altitude of elves was 87.1 km with 50% of observations between 85.2 and 88.6 km. However, there is significant night-to-night variation as well as a possible trend over the years. The night with the lowest elves featured a mean of 83.4 km and the night with the highest a mean of 90.0 km during the winter season. One summer night case (20 August 2010) with elves near 93.3 km altitude falls at the end of the tail of the elve altitude distribution. This may be an unusual case where a modification in the electron density gradient is produced at a higher altitude, perhaps associated with electron depletion below sporadic E [*Lehmacher et al*., 2015]. Remarkable is that the winters of 2014 to 2016 contributed mainly low elves (~84 km), bringing down the average height from 87.8 km of the years before. A link with the solar cycle and geomagnetic disturbances is likely present as we found ap-index >10 in the reduced altitude cases while it was 0-5 in the normal altitude cases.

Changes of 1–3 km in elve heights are observed in individual nights over time spans of 0.5–2 hours, in agreement with the findings of *Han and Cummer* [2010] and *Lay and Shao* [2011]. This suggests the nocturnal evolution of altitude may occur as a result of long period neutral density and

temperature changes (gravity waves and tides), or perhaps changes in meteoric dust particles [e.g. *Friedrich et al.,* 2012] or chemical factors altering the electron density gradient. Observed altitudes change at different moments during most elve nights, and may decrease or increase regardless of the time. Note that in case of gravity waves as cause, these must have a wavelength much longer than those that show up as bands and ripples within the elve disk [*van der Velde et al*., 2011; *Yue and Lyons*, 2015]. The effect of large scale gravity waves can be to bring down and replace the D-region electron gradient [*Sugiyama*, 1988]. Some of the long period changes may be due to tides. These are known to increase O and OH airglow and to slightly lower their peak altitudes after 3 a.m. local time in midwinter [e.g. *Zhang and Shepherd*, 1999]. We do not see consistent lowering of elves after that time, however: in 2 nights (*d* and *e* in Figure 3) this might be the case, in one night (*a*) we actually see an increase, and other nights did not have sufficient numbers of elves late in the night. It can be noted that statistics of radiowave tweek reflection heights only show slightly increased altitudes (<1 km) at the beginning as well as the end of the night [*Ohya et al.*, 2011].

One may assume [*Wu et al.,* 2014] that a connection exists between OH and the electron density profile with possible roles for atomic oxygen, nitric oxide, cluster hydrates and meteoric dust particles. What needs to be established better is whether OH airglow and elves really occur simultaneously at the same altitude, and whether airglow and radiowave reflection heights are correlated.

This study provides the most precise elve emission height statistics to date and reveals some of its variability at the time scale of years, seasons, individual nights and hours. We hope this will be instrumental in solving links between physical processes in the upper mesophere – lower ionosphere region.

Acknowledgments

This study was supported by research grants from the Spanish Ministry of Economy and Competitiveness (MINECO) and the European Regional Development Fund (ERDF): AYA2009-14027-C05-05, AYA2011-29936-C05-04, ESP2013-48032-C5-3-R and ESP2015-69909-C5-5-R. The analysis of two cases with summer elves was possible thanks to the availability of the camera system on Pic du Midi, installed and maintained by Serge Soula and the Observatoire Midi-Pyrénées. We are grateful to Hans Betz and Matthias Möhrlein of nowcast GmbH who provided us with Linet data. We thank the International Reference Ionosphere website as well as the observatories, GFZ Potsdam, the INTERMAGNET network and ISGI (isgi.unistra.fr) for making the geomagnetic indices available. Images used for this study are available from the authors (OV). Other data are supplied as detailed in the Supporting Information section.

References

Baker, D. J., and J. A. T. Stair (1988), Rocket measurements of the altitude distributions of the hydroxyl airglow, Phys. Scr., 37, 611–622, doi:10.1088/0031-8949/37/4/021.

Barrington-Leigh, C. P., and U. S. Inan (1999), Elves triggered by positive and negative lightning discharges, Geophys. Res. Lett., 26, 683–686, doi:10.1029/1999GL900059.

Barrington□Leigh, C., U. Inan, and M. Stanley (2001), Identification of sprites and elves with intensified video and broadband array photometry, J. Geophys. Res., 106(A2), 1741-1750.

Boeck, W. L., O. H. Vaughan, R. Blakeslee, B. Vonnegut, and M. Brook (1992), Lightning induced brightening in the airglow layer, Geophys. Res. Lett., 19, 99–102.

Betz, H.-D., K. Schmidt, P. Oettinger, and M. Wirz (2004), Lightning detection with 3-D discrimination of intracloud and cloud-to-ground discharges, Geophys. Res. Lett., 31, L11108, doi:10.1029/2004GL019821.

Betz, H. D., K. Schmidt, P. Laroche, P. Blanchet, W. P. Oettinger, E. Defer, Z. Dziewit, J. Konarski (2009), LINET—An international lightning detection network in Europe, Atm. Res., 91, 2–4, 564-573, doi: 10.1016/j.atmosres.2008.06.012.

Blaes, P. R., R. A. Marshall, and U. S. Inan (2014), Return stroke speed of cloud-to-ground lightning estimated from elve hole radii, Geophys. Res. Lett., 41, 9182–9187, doi:10.1002/2014GL062392.

Blaes, P. R., R. A. Marshall, and U. S. Inan (2016), Global occurrence rate of elves and ionospheric heating due to cloud-to-ground lightning, J. Geophys. Res. Space Physics, 121, 699–712, doi:10.1002/2015JA021916.

Bór, J., 2013: Optically perceptible characteristics of sprites observed in Central Europe in 2007-2009. J. Atmos. Sol. Terr. Phys., 92, 151-177 doi.org/10.1016/j.jastp.2012.10.008.

Chen, A. B., et al. (2008), Global distributions and occurrence rates of transient luminous events, J. Geophys. Res., 113, A08306

Chen, A. B.-C., H.-T. Su, and R.-R. Hsu (2014), Energetics and geographic distribution of elve-producing discharges, J. Geophys. Res. Space Physics, 119, 1381–1391, doi:10.1002/2013JA019470.

Cho, Y.-M., and G. G. Shepherd (2006), Correlation of airglow temperature and emission rate at Resolute Bay (74.68 N), over four winters (2001 – 2005), Geophys. Res. Lett. , 33, L06815, doi:10.1029/2005GL025298

Friedrich, M. and K. M. Torkar (2001), FIRI: A semi-empirical model of the lower ionosphere., J. Geophys. Res., 106, 21409–21418.

Friedrich, M., M. Rapp, T. Blix, U.-P. Hoppe, K. Torkar, S. Robertson, S. Dickson, and K. Lynch (2012), Electron

384 loss and meteoric dust in the mesosphere, Ann. Geophys., 30, 1495-1501, doi:10.5194/angeo-30-1495-2012.
385
386 Fukunishi, H., Y. Takahashi, M. Kubota, K. Sakanoi, U. S. Inan, and W. A. Lyons (1996), Elves: Lightning-
387 induced transient luminous events in the lower ionosphere, Geophys. Res. Lett., 23, 2157–2160,
388 doi:10.1029/96GL01979.
389
390 Füllekrug M., A. Mezentsev, S. Soula, O. van der Velde, and T. Farges (2013), Sprites in low-frequency radio
391 noise, Geophys. Res. Lett., 40, 2395–2399, doi:10.1002/grl.50408.
392
393 Gordillo-Vázquez, F. J., A. Luque, and C. Haldoupis (2016), Upper D region chemical kinetic modeling of LORE
394 relaxation times, J. Geophys. Res. Space Physics, 121, doi:10.1002/2015JA021408.
395
396 Haldoupis, C., M. Cohen, B. Cotts, E. Arnone, and U. Inan (2012), Long-lasting D-region ionospheric
397 modifications, caused by intense lightning in association with elve and sprite pairs, Geophys. Res. Lett., 39, L16801,
398 doi:10.1029/2012GL052765.
399
400 Han, F., and S. A. Cummer (2010), Midlatitude nighttime D region ionosphere variability on hourly to monthly
401 time scales, J. Geophys. Res., 115, A09323, doi:10.1029/2010JA015437
402
403 Huang, T.-Y., C. L. Kuo, C. Y. Chiang, A. B. Chen, H. T. Su, and R. R. Hsu (2010), Further investigations of
404 lightning□induced transient emissions in the OH airglow layer, J. Geophys. Res., 115, A10326,
405 doi:10.1029/2010JA015558.
406
407 Inan, U. S., T. F. Bell, and J. V. Rodriguez (1991), Heating and ionization of the lower ionosphere by lightning,
408 Geophys. Res. Lett., 18(4), 705–708.
409
410 Inan, U. S., W. A. Sampson, and Y. N. Taranenko (1996), Space□time structure of optical flashes and ionization
411 changes produced by lightning□EMP, Geophys. Res. Lett., 23(2), 133–136.
412
413 Israelevich, P. L., Y. Yair, A. D. Devir, J. H. Joseph, Z. Levin, I. Mayo, M. Moalem, C. Price, B. Ziv, and A.

414 Sternlieb (2004), Transient airglow enhancements observed from the space shuttle Columbia during the MEIDEX sprite
415 campaign, Geophys. Res. Lett., 31, L06124, doi:10.1029/2003GL019110.
416
417 Kuo, C.-L., et al. (2007), Modeling elves observed by FORMOSAT-2 satellite, J. Geophys. Res., 112, A11312,
418 doi:10.1029/2007JA012407.
419
420 Kuo, C. L., et al. (2012), Full-kinetic elve model simulations and their comparisons with the ISUAL observed
421 events, J. Geophys. Res., 117, A07320, doi:10.1029/2012JA017599.
422
423 Lay, E. H., and X.□M. Shao (2011), High temporal and spatial□resolution detection of D□layer fluctuations by
424 using time□domain lightning waveforms, J. Geophys. Res., 116, A01317, doi:10.1029/2010JA016018.
425
426 Lehmacher, G. A., Larsen, M. F., and Croskey, C. L.: Observation of electron biteout regions below sporadic E
427 layers at polar latitudes, Ann. Geophys., 33, 371-380, doi:10.5194/angeo-33-371-2015, 2015.
428
429 López-González, M. J., et al., (2005), Tidal variations of O2 Atmospheric and OH(6-2) airglow and temperature at
430 mid-latitudes from SATI observations, Annales Geophysicae, 23, 3579–3590.
431
432 Marshall, R. A., U. S. Inan, and V. S. Glukhov (2010), Elves and associated electron density changes due to
433 cloud□to□ground and in□cloud lightning discharges, J. Geophys. Res., 115, A00E17
434
435 Maurya, A. K., B. Veenadhari, R. Singh, S. Kumar, M. B. Cohen, R. Selvakumaran, S. Gokani, P. Pant, A. K.
436 Singh, and U. S. Inan (2012), Nighttime D region electron density measurements from ELF-VLF tweek radio
437 atmospherics recorded at low latitudes, J. Geophys. Res., 117, A11308, doi:10.1029/2012JA017876.
438
439 Montanyà, J., O. van der Velde, D. Romero, V. March, G. Solà, N. Pineda, M. Arrayas, J. L. Trueba, V. Reglero,
440 and S. Soula (2010), High-speed intensified video recordings of sprites and elves over the western Mediterranean Sea
441 during winter thunderstorms. J. Geophys. Res.,115, A00E18, doi:10.1029/2009JA014508.
442
443 Montanyà, J., Fabró, F., van der Velde, O., March, V., Williams, E. R., Pineda, N., Romero, D., Solà, G., and

444 Freijo, M. (2016): Global Distribution of Winter Lightning: a threat to wind turbines and aircraft, Nat. Hazards Earth
445 Syst. Sci. Discuss., doi:10.5194/nhess-2015-302.
446
447 Neubert, T., et al. (2008), Recent results from studies of electric discharges in the mesosphere, Surv. Geophys,
448 29(2), 71–137, doi:10.1007/s10712-008-9043-1.
449
450 Newsome, R. T. and U. S. Inan (2010), Free□running ground□based photometric array imaging of transient
451 luminous events , J. Geophys. Res. , 115 , A00E41
452
453 Ohya, H., K. Shiokawa, and Y. Miyoshi (2011), Long-term variations in tweek reflection height in the D and
454 lower E regions of the ionosphere, J. Geophys. Res., 116, A10322, doi:10.1029/2011JA016800.
455
456 Reid, G. C. (1970), Production and loss of electrons in the quiet daytime D region of the ionosphere, J. Geophys.
457 Res., 75(13), 2551–2562, doi:10.1029/JA075i013p02551.
458
459 Said, R. K., M. B. Cohen, and U. S. Inan (2013), Highly intense lightning over the oceans: Estimated peak
460 currents from global GLD360 observations, J. Geophys. Res. Atmos., 118, 6905–6915, doi:10.1002/jgrd.50508
461
462 Shao, X.-M., E. H. Lay, and A. R., Jacobson (2013): Reduction of electron density in the night-time lower
463 ionosphere in response to a thunderstorm, Nature Geoscience, 6, 29–33, doi: 10.1038/ngeo1668
464
465 Soula, S., O. van der Velde, J. Montanya, T. Neubert, O. Chanrion, and M. Ganot (2009), Analysis of
466 thunderstorm and lightning activity associated with sprites observed during the EuroSprite campaigns: Two case
467 studies, Atmos. Res., 91, 514–528, doi:10.1016/j.atmosres.2008.06.017.
468
469 Soula, S., O. van der Velde, J. Palmieri, J. Montanya, O. T. Neubert, F. Gangneron, Y. Meyerfeld, F. Lefeuvre,
470 and G. Lointier (2010), Characteristics and conditions of production of transient luminous events observed over a
471 maritime storm, J. Geophys. Res., 115, D16118, doi:10.1029/2009JD012066.
472
473 Soula, S., F. Iacovella, O. van der Velde, J. Montanyà, M. Füllekrug, T. Farges, J. Bór, J.-F. Georgis, S. NaitAmor,

474 and J.-M. Martin (2014), Multi-instrumental analysis of large sprite events and their producing storm in southern
475 France, Atmos. Res., doi: 10.1016/j.atmosres.2012.10.004
476
477 Takahashi, Y., R. Miyasato, T. Adachi, K. Adachi, M. Sera, A. Uchida, H. Fukunishi (2003), Activities of sprites
478 and elves in the winter season, Japan, Journal of Atmospheric and Solar-Terrestrial Physics, 65, pp. 551–560
479
480 Taranenko, Y. N., U. S. Inan, and T. F. Bell (1993), The interaction with the lower ionosphere of electromagnetic
481 pulses from lightning: Excitation of optical emissions, Geophys. Res. Lett., 20(23), 2675–2678.
482
483 van der Velde, O. A. (2008), Morphologie de sprites et conditions de productions de sprites et de jets dans les
484 systèmes orageux de méso-échelle, PhD dissertation, Université de Toulouse III – Paul Sabatier, Toulouse, France.
485
486 van der Velde, O. A., J. Montanya, M. Fullekrug, and S. Soula (2011), Gravity waves, meteor trails, and
487 asymmetries in Elves, XIV International Conference on Atmospheric Electricity, August 08–12, 2011, Rio de Janeiro,
488 Brazil. doi: 10.13140/RG.2.1.1481.8645
489
490 van der Velde, O. A., J. Montanyà, S. Soula, N. Pineda, and J. Mlynarczyk (2014), Bidirectional leader
491 development in sprite-producing positive cloud-to-ground flashes: Origins and characteristics of positive and negative
492 leaders, J. Geophys. Res. Atmos., 119, 12,755–12,779, doi:10.1002/2013JD021291.
493
494 Wu, Y. J., Williams, E. R. and Hsu, R. R. (2014), The D-Region Ledge at Nighttime: Why are Elves Collocated
495 with the OH Meinel Band Airglow Layer?, AGU Fall Meeting 2014, abstract AE31B-3408
496
497 Yair, Y. (2009), From the MEIDEX to the ILAN winter campaigns: results from 6 years of sprite research in
498 Israel. Proceedings Chapman Conference on the effects of thunderstorms and lightning in the upper atmosphere, p 12,
499 Penn-State University, State College, PA, (10-14 May 2009).
500
501 Yue, J., and W. A. Lyons (2015), Structured elves: Modulation by convectively generated gravity waves, Geophys.
502 Res. Lett., 42, doi:10.1002/2014GL062612.
503

Zhang, S. P., and G. G. Shepherd (1999), The influence of the diurnal tide on the O(1S) and OH emission rates observed by WINDII on UARS, Geophys. Res. Lett., 26, 529–532, doi:10.1029/1999GL900033.

510 **Figure captions**

511

512 **Figure 1.** a) Boxplot of the peak current of Linet-detected cloud-to-ground strokes for those elves whose altitude
513 has been determined. b) Map with locations of detected strokes which produced elves observed from 2008-2016 by the
514 camera in northeastern Spain (blue triangle) and Pic du Midi (black triangle). The color indicates the elve altitude
515 according to the histogram. Black dots are Linet detections for confirmed elves without the possibility of optical
516 verification of the stroke locations. c) Histogram of the altitudes of the events shown on the map.

517

518 **Figure 2.** Variability of individual elve altitudes and the 95% confidence interval (bounded by red triangles) of the
519 mean altitude for nights with elves observed from northeastern Spain. The two nights at the bottom indicated by stars
520 are cases of summer elves obtained by the camera at Pic du Midi. The label refers to the 00 UTC date of the night.
521 Labels marked in grey indicate nights when geomagnetic ap-index > 10 nT. The vertical dashed line indicates the mean
522 elve altitude.

523

524 **Figure 3.** Altitudes of individual elves over time and space (distance from the camera).

a)

b)

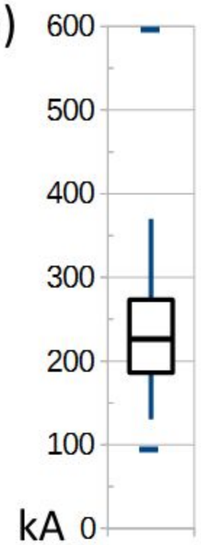

Bay of Biscay

France

Atlantic Ocean

Spain

Balearic Sea

Mediterranean Sea

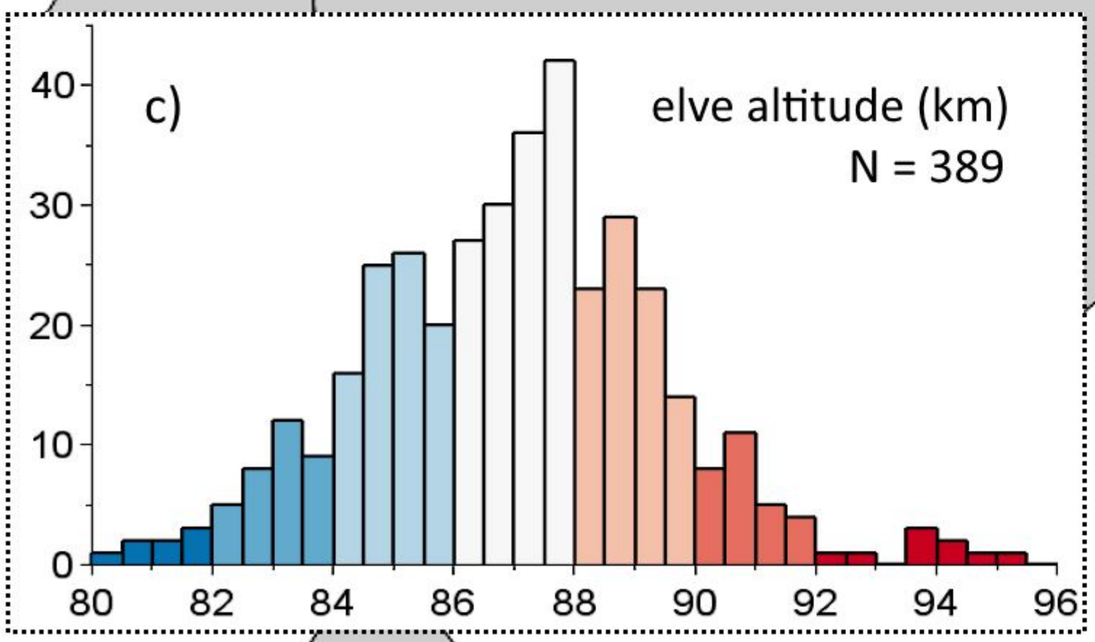

altitude (km)

80 82 84 86 88 90 92 94 96

24 Nov 2008
27 Nov 2008
3 Dec 2008
11 Dec 2008
21 Jan 2009
8 Feb 2009
5 Nov 2009
8 Nov 2009
9 Nov 2009
1 Dec 2009
1 Jan 2010
10 Jan 2010
20 Feb 2010
26 May 2010
10 Nov 2010
29 Nov 2010
2 Dec 2010
3 Dec 2010
21 Jan 2011
1 Mar 2011
28 Jun 2011
5 Dec 2012
25 Jan 2013
3 Feb 2013
7 Feb 2013
27 Feb 2013
22 Nov 2013
25 Nov 2013
26 Dec 2013
28 Jan 2014
9 Feb 2014
5 Nov 2014
17 Jan 2015
6 Jan 2016
12 Jan 2016
*20 Aug 2010
*7 Jun 2015
[ap > 10]

80 82 84 86 88 90 92 94 96

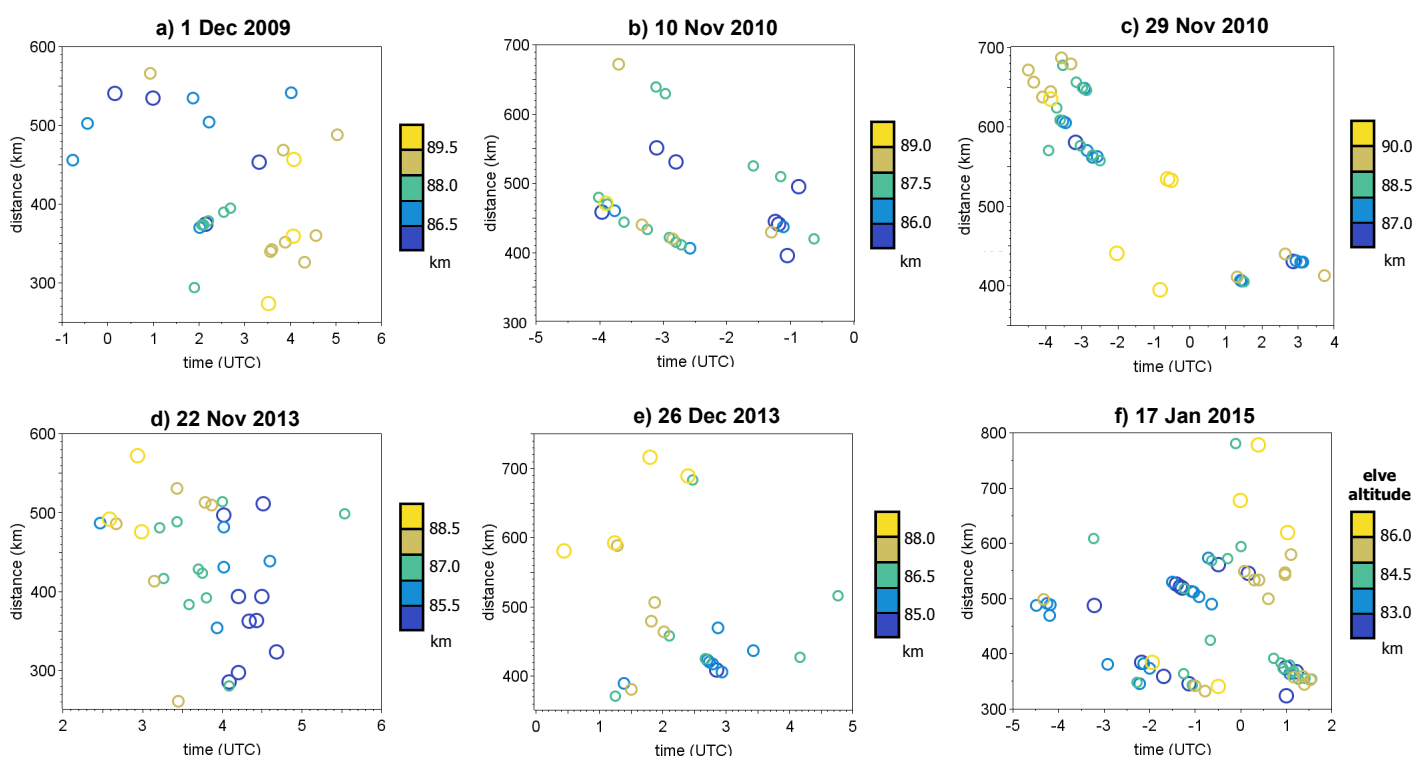
a) 1 Dec 2009
b) 10 Nov 2010
c) 29 Nov 2010
d) 22 Nov 2013
e) 26 Dec 2013
f) 17 Jan 2015
distance (km)
time (UTC)
km
elve altitude

Geophysical Research Letters

Supporting Information for

Statistics and variability of the altitude of elves

Oscar A. van der Velde and Joan Montanyà

Lightning Research Group, Electrical Engineering Department, Technical University of Catalonia.

Colon 1, 08222 Terrassa (Barcelona), Spain

Contents of this file

Additional Supporting Information

available at www.lightningwizard.com/research/GRL_elve_altitudes.7z

Linet location data was reduced to two decimals. Full data can be obtained from Nowcast GmbH (H.-D. Betz, nowcast.de).

Introduction

We include here in Text S1 the calculation for event altitude from an elevation angle determined by means of the star fit software combined with the known great circle distance to the triggering cloud-to-ground stroke. In Text S2 we detail the steps followed to obtain elve altitudes. Text S3 provides one elve example with resulting altitude estimate from two cameras. Figure S4 shows how elve altitude varies over the night.

Text S1.

In order to calculate the altitude of a sprite, jet, elve or an object above the Earth's curved surface, its great circle distance d must be known, and from the images and star fitting method the elevation angle A^0 is derived. The Earth is an oblate sphere with a radius 6356 km < R < 6378 km. For the calculations we assume it is a true sphere, which is, given the only <0.3% differences, good enough for the comparatively short distances of the events. The above schematic picture exaggerates the height and distance of the event compared to the Earth.

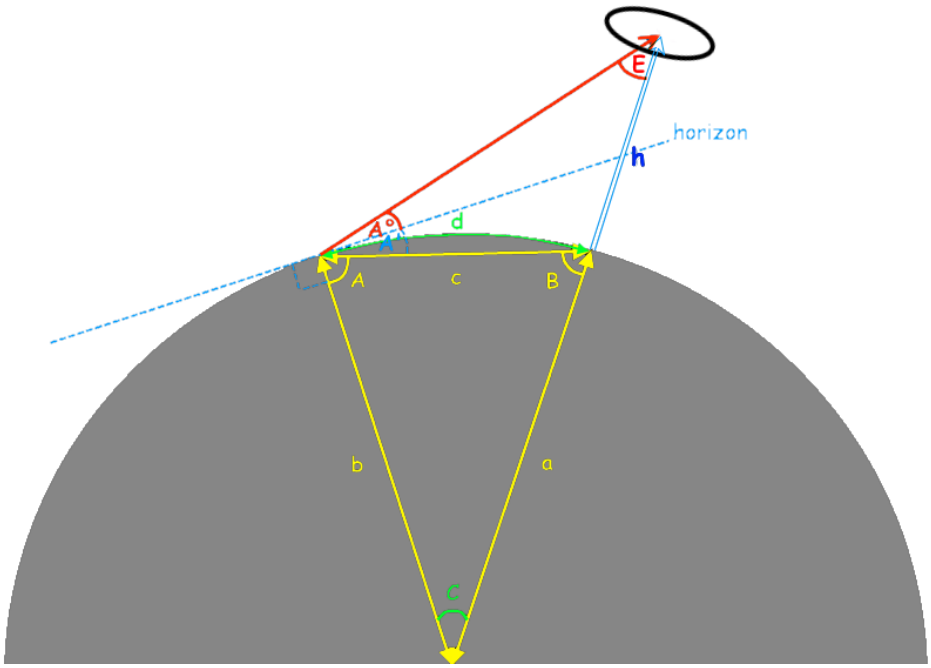

Figure S1. Geometry for the calculation of event altitude h based on great circle distance d and observed elevation angle A^0.

The transient luminous event occurs in the zenith above point B at a great circle distance d from the camera in A. The astronomical software yields the elevation angle A^0 to the center of the elve above the astronomical horizon, which is tangent to the Earth's curved surface in A. If an elevation angle

would have been derived as a difference from a visible horizon from a mountain or balloon camera location, one would have to consider this (a calculation different from described here, though perhaps not with significantly different results).

We can now construct a triangle ABC. Angle C (in degrees) follows simply from d:

$$C=\frac{180}{\pi}\frac{d}{a} \quad \text{with} \quad a=R$$

The cosine rule for triangle ABC with sides abc opposite to the corresponding corners ABC goes:

$$c^2=a^2+b^2-2ab\cos C$$

so if $a=b$ it simplifies to

$$c=\sqrt{2a^2-2a^2\cos C}$$

which can be used for determining the second triangle: ABE. We happen to know more about the corners of this triangle, because the sum of A and A' is 90°, and the sum of ABC is 180°. So:

$$A=B=\frac{180°-C}{2}=90°-\frac{1}{2}C \qquad \text{and} \qquad A'=90°-A=\frac{1}{2}C$$

While corner E can be derived from the large triangle ACE:

$$S=180°-C-\left(90°+A^0\right)=90°-C-A^0$$

We can now solve the triangle ABE with the sine rule:

$$\frac{\sin A}{a}=\frac{\sin B}{b}=\frac{\sin C}{c}$$

Filling this out with the corresponding sides and angles gives:

$$\frac{\sin\left(A^0+A'\right)}{h}=\frac{\sin E}{c}$$

and the height of the TLE is found:

$$h=\frac{c\sin\left(A^0+\frac{1}{2}C\right)}{\sin\left(90°-C-A^0\right)}$$

If h_{cam} is not zero, we have to deal with this from the first step.

$a = R + h_{cam}$

Points A and B are then above the Earth's surface, which requires a correction of great circle distance d which was measured over the surface itself. The corrected d' is:

$$\frac{d'}{2\pi(R+h_{cam})} = \frac{d}{2\pi R} \qquad \text{so} \qquad d' = \frac{(R+h_{cam})}{R} d$$

By using the corrected a and d' the same calculation is performed, and h_{cam} is added to the final answer h.
Running a test calculation for typical TLE distances, it becomes obvious that the differences between d and c, as well as d and d', are really small: less than 0.1 km, which is perhaps only a half percent of the distance. The uncertainty in the precise distance is larger than that imposed by the calculation when angle C is small (commonly less than 6° of latitude/longitude for TLE observed from ground).
It is therefore possible to simplify the calculation to:

$$h = \frac{d \sin(A^0 + \frac{1}{2}C)}{\sin(90° - C - A^0)} + h_{cam}$$

avoiding the calculation of c, and involves only an initial calculation of angle C.

Note that the software SkyCharts (Cartes du Ciel) calculates the atmospheric refraction and scales its elevation grid accordingly.

Text S2.

The steps taken to reproduce the results of this study are described here.

1) Observation with camera system described in the paper. UFOCapture V2/HD setting details for elves can be obtained by contacting the author (OV). The most important setting is Detect Level Noise tracking <100 and MinL-N between -3 to -1 setting a sensitive brightness difference threshold.
2) The video clips obtained contain about 20 frames. They are processed to separate event (background subtracted) and background sky. The resulting images are available for research purposes (personal database of the author OV).
3) Images have black borders and PAL aspect ratio. Batch cropping and resizing and output as BMP files was done in Irfanview 4.38. The following settings result in the best match with star fields: CROP: X-pos

6, Y-pos 0, Width 703, Height 576. RESIZE 760x576 (if e.g. 768x576 there will be a horizontal or vertical mismatch with stars)

4) Using Sky Charts - Cartes du Ciel v2.76c from www.stargazing.net /astropc (not v3 which accepts only FITS images):
   a) Make sure to set Preferences... Observatory (obtain from authors) and Date/Time for the event in UTC (+0). Projection: “ARC”.
   b) Aim in the roughly good direction (WNW for Atlantic, SE for Mediterranean)
   c) Load Images: Background image... and select the background sky image.
   d) Make sure there is an “eyepiece” to assist in star aiming and increase/decrease the number of visible stars.
   e) Set the correct field of view, e.g. Search – Locate new position... and go for Field Width 31° 15' for the 12mm lens.
   f) Find stars in the software matching those in the image. It can be tricky at first. Move around by rightclicking (Center) where the center of the view should be next. Images: Blinking image helps.
   g) Fine-tune the match by right-clicking in small steps near the Eyepiece the amount of shift between software and image stars. Perhaps the view needs adjustment (if lens properties not tuned before).
   h) Tune the Search – Locate new position... Orientation to rotate horizon.
   i) When stars overlap precisely the ones in the image, save the configuration as a CDC file.
   j) Now load the corresponding elve image without changing any parameters. Select Blinking image to remove the software projected stars, grids, etc. Point at the center of the elve, take note of the elevation in the info bar. Do this a few times then write down the most encountered Az/Ele values.
   k) Repeat for next elve images – check if the background still fits the stars when time is adjusted to the next event. If so, just read out the elve center.
5) With obtained Azimuth and Elevation take the lightning stroke location at the time of the elve into a simple great circle calculator (http://williams.best.vwh.net/gccalc.htm will do, use spherical Earth). Set the observation site as first point, the stroke as the second, calculate the distance and azimuth.
6) Reject the stroke if azimuth does not match starfix-obtained one within 1 degree or if lateral stroke distance greater than 10 km. Try an alternative stroke if available within 20 ms of this event.
7) Use a calculation spreadsheet/script (can be obtained from the authors) to input elve elevation and stroke great circle distance and find the corresponding elve altitude.
8) The sheet with elve altitudes, strokes, times and dates, and the stroke error obtained by the authors is provided in a zipped file available at the link provided on the first page, or it can be obtained from the authors.
9) The altitudes should be corrected for the effects of viewing perspective by a simple procedure, assuming the elve hole to be 35 km wide. The

script is included. As elves usually occur at 5-15° above the horizon, the use of great circle distance instead of direct distance through the air amounts only to -0.1 km in altitude.

Text S3.

As a demonstration of the precision of the height calculation method, we apply the procedure outlined in S2 to an elve (1 December 2010, 230619 UTC) observed simultaneously at the camera sites of Observatoire du Pic du Midi (42.94°N, 0.14°E, 2880m) and Sant Vicenç de Castellet (41.67°N, 1.86°E, 190m). A +250 kA stroke was detected by Linet at the location 39.8702°N 3.5136°E, halfway between the islands Mallorca and Menorca in the Mediterranean Sea. All calculations assume a spherical Earth with a local radius of 6368 km.

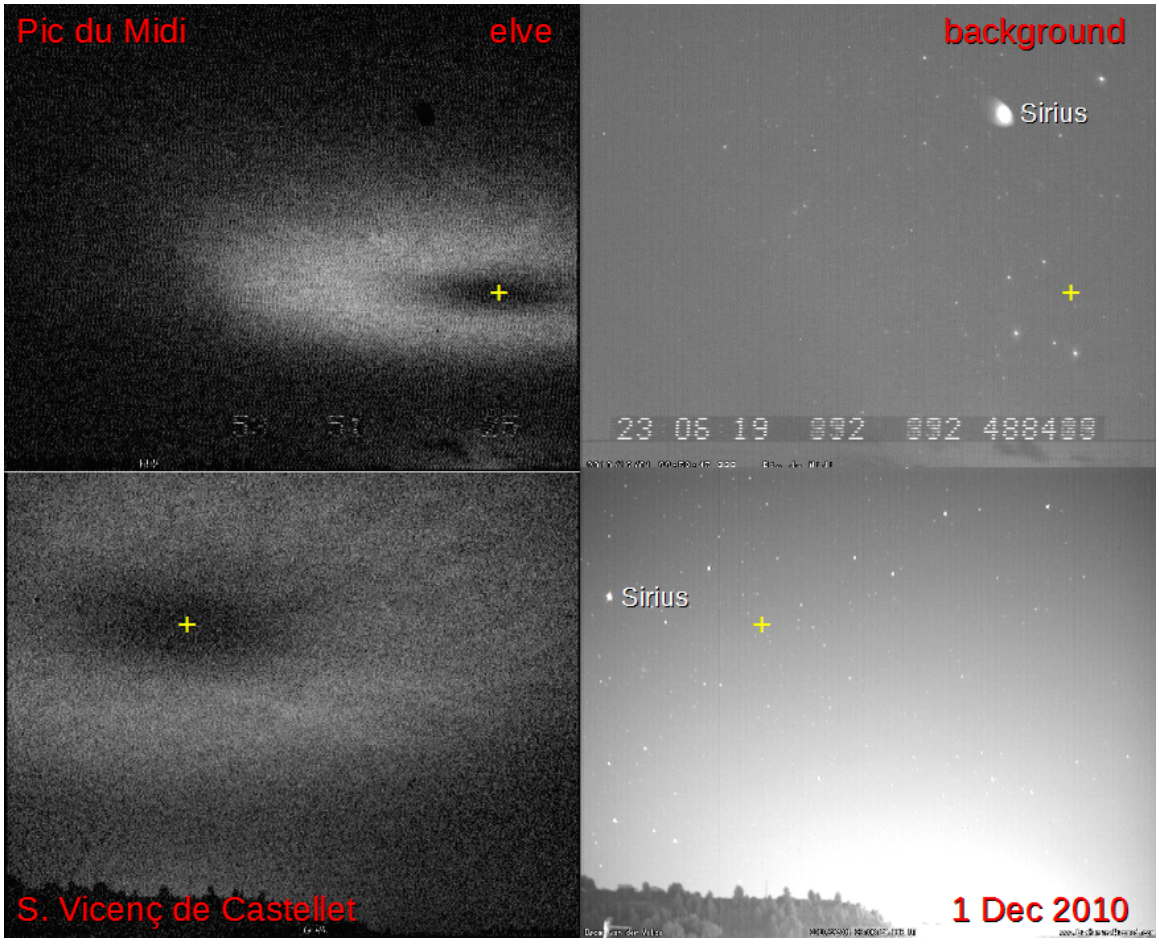

Figure S3. Elve event-only and background images (brightness was mulltiplied by 3), observed simultaneously from two camera locations. The approximate elve centers are marked. After fixing the stars in the background image in Cartes du Ciel v2.76, the resulting center values were read out and presented in Table S3.

Table S3. Elve altitude calculated from the optical analysis and Linet return stroke location.

	Azimuth	Elevation	Stroke distance	Resulting altitude	Perspective-corrected altitude
S. Vicenç C.	145.2°	18°52'	243.61 km	89.3 km	88.0
Pic du Midi	140.1°	8°57'	441.68 km	88.9 km	88.4

Text S4.

The peak current in Linet data corresponding to the unusual elve-producing strokes shows no correlation with elve altitude (Figure S4). Peak current does show some correlation with subjective elve brightness in a comparison we performed on a limited number of events (not shown here), so we consider the absence of correlation real.

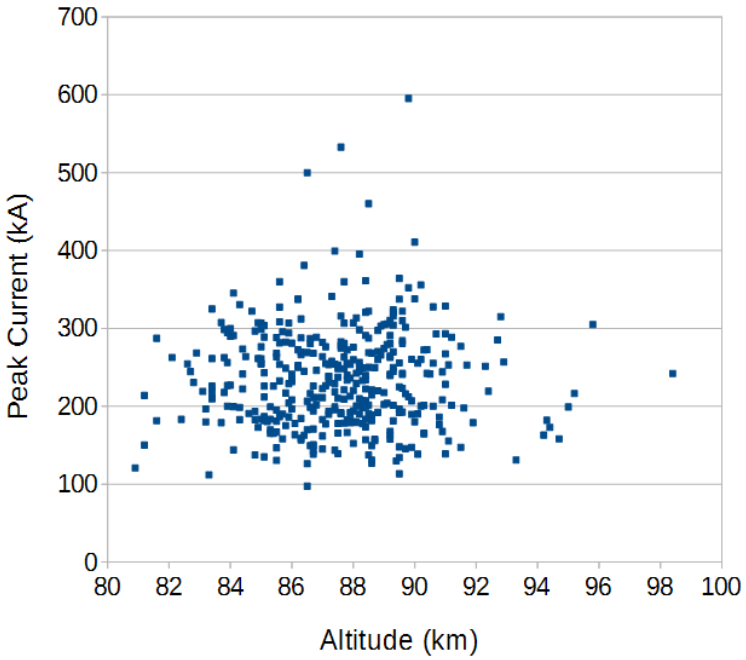

Figure S4. Linet peak current versus elve altitude (strokes <70 kA filtered out as those are unlikely to be detections of the main stroke)

Text S5.

Elve altitude variation with time is strongly dominated by the mean altitudes of individual nights, so no clear relation shows (unless 2014-2016 nights are removed, but even then there are too few elves and contributing elve nights per time interval to find statistical significance).

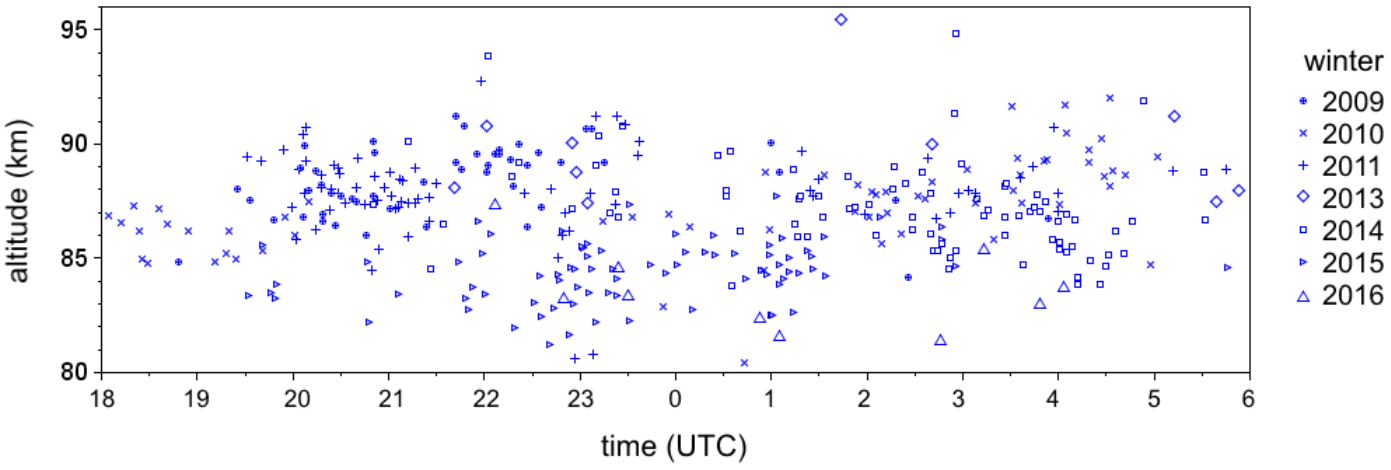

Figure S5. Elve altitude with time, grouped by year (e.g. "2009" is Nov 2008-Feb 2009).

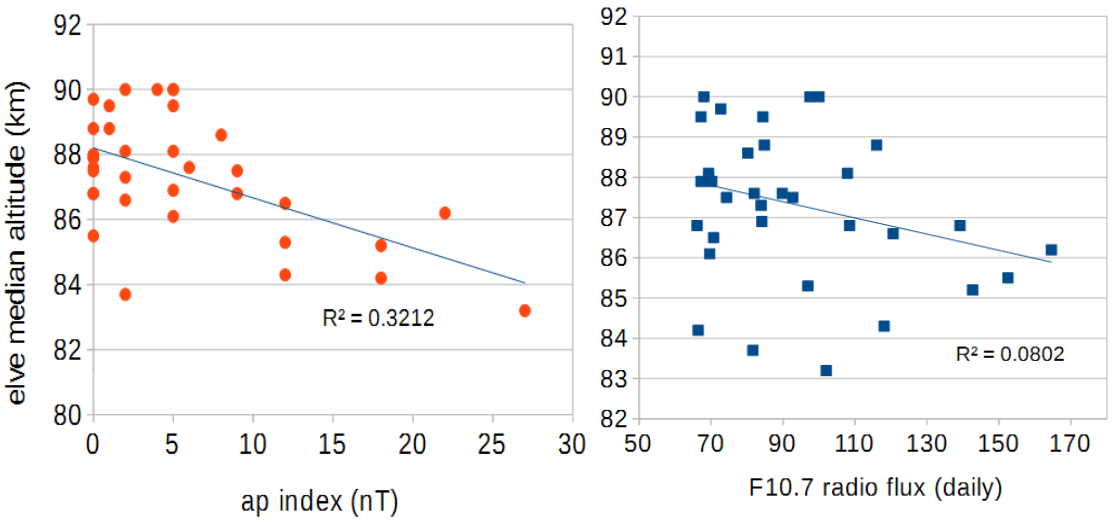

Figure S6. Scatterplots for elve median altitude per night (35 nights) and the ap-index, as well as the F10.7 daily solar radio flux.